https://doi.org/10.5194/egusphere-2025-2939
Preprint. Discussion started: 8 July 2025

Impact of Cloud Vertical Structure Perturbations on the Retrieval of Cloud Optical Thickness and Effective Radius from FY4A/AGRI

Jing Sun[1,2], Yunying Li[1,3], Hao Hu[4], Qian Li[1, 3], Chengzhi Ye[5], Yi-ning Shi[4], Zitong Chen[1]

1 College of Meteorology and Oceanography, National University of Defense Technology, Changsha 410073, China
2 China Meteorological Administration Basin Heavy Rainfall Key Laboratory/Hubei Key Laboratory for Heavy Rain Monitoring and Warning Research, Institute of Heavy Rain, China Meteorological Administration，Wuhan 430205, China
3 Key Laboratory of High Impact Weather(special), China Meteorological Administration, Changsha 410073, China
4 State Key Laboratory of Severe Weather Meteorological Science and Technology, CMA Earth System Modeling and Prediction Centre, Beijing 100081, China
5 Institute of Meteorological Sciences of Hunan Province, Hunan Meteorological Bureau, Changsha 410118, China

Correspondence to: Yunying Li (ghlyy@mail.iap.ac.cn)

Abstract. The vertical structure of clouds plays a critical role in atmospheric radiative transfer processes and is a major source of uncertainty in satellite-based retrievals of cloud optical thickness (COT) and cloud effective radius (CER). This study develops a retrieval model for COT and CER based on a random forest framework coupled with spatial gradient features, using multispectral observations from the FY4A/AGRI (Advanced Geostationary Radiation Imager) and simulations from Advanced Radiative Transfer Modeling System (ARMS) over central and eastern China during June–August 2018. The retrieval results agree well with MODIS, with correlation coefficients of 0.87 and 0.91 for COT and CER, respectively. To assess the impact of vertical cloud structure, ten sensitivity experiments varied water and ice content in different cloud layers. The results indicate that upper-level ice clouds significantly mask reflectance from lower clouds, reducing total reflectance by approximately 50%, leading to lower retrieved values than those of single-layer clouds. For CER < 20 μm, the mean COT increase due to low- and mid-level water cloud variations in single-layer clouds exceeds that in double-layer clouds by about 24%, primarily due to the masking effect of upper-level ice clouds in double-layer structures. This masking also contributes to retrieval biases in three-layer cloud systems. Furthermore, increased mid-level liquid water enhances the nonlinear relationship between COT and CER, increasing retrieval

https://doi.org/10.5194/egusphere-2025-2939
Preprint. Discussion started: 8 July 2025

uncertainties. This study highlights the importance of considering multi-layer cloud structures in remote sensing algorithms and radiative transfer models.

1 Introduction

Clouds cover approximately 67% of the Earth's surface on average (Fang et al., 2016) and exert a pivotal influence on the evolution of weather systems and the global hydrological cycle (Matus et al., 2017). The pronounced spatial heterogeneity of clouds introduces substantial uncertainties in their microphysical properties, which is turn complicates the interactions between clouds and radiation. This uncertainty remains a critical limitation in the accuracy of climate change projections and the performance of numerical weather prediction models (IPCC, 2021). The radiative characteristics of clouds are highly sensitive to the physical attributes of cloud particles, particularly variations in key parameters including cloud effective radius (CER), cloud optical thickness (COT), cloud water content, cloud top height, and cloud base height (Wang et al., 2018; Letu et al., 2020). Among these, COT and CER are two important cloud microphysical parameters that govern the cloud's ability to scatter and absorb solar radiation.

With the advancement of satellite technology, satellite observations have become a powerful tool for capturing the spatial and temporal variations of COT and CER on both regional and global scales (Zhao et al., 2018). As a result, the retrieval of COT and CER from satellite data has attracted increasing attention. A widely used approach is the classic bispectral reflectance technique, which assumes that the cloud within each satellite pixel is single-phase and vertically homogeneous. By using reflectance measurements from a non-absorbing channel that is primarily sensitive to COT and an absorbing channel sensitive to both COT and CER, it is possible to retrieve their effective values (Nakajima and King, 1990). This principle underlies many operational cloud optical and microphysical products derived from spectral imagers such as MODIS, AHI, and AGRI (Platnick et al., 2003; Min et al., 2017; Letu et al., 2020; Chen et al., 2020; Zhuge et al., 2021; Liu et al., 2023). The accuracy of these retrievals largely depends on the precision of radiative transfer modeling and the adequacy of cloud optical property characterization. Radiative transfer models simulate the top-of-atmosphere radiance observed by satellites by accounting for atmospheric absorption, scattering, and emission processes under various meteorological conditions, and thus serve as the physical foundation for developing satellite-based cloud retrieval algorithms (RTTOV: Saunders et al., 2018; CRTM: Chen et al., 2008; ARMS: Weng et al., 2020).

Given the complex structure of atmospheric clouds and the computational cost of radiative transfer simulations in cloudy atmospheres, most current cloud retrieval algorithms adopt a simplified assumption

https://doi.org/10.5194/egusphere-2025-2939
Preprint. Discussion started: 8 July 2025

of a "single-layer homogeneous cloud." In reality, clouds are often composed of multiple vertically arranged layers, each characterized by unique microphysical features including phase type, droplet size variability, and spatial structure. Based on combined CALIPSO and CloudSat observations, Li et al. (2011) reported that overlapping clouds occur with a global probability of up to 25.8%. Similarly, Yuan and Oreopoulos (2013) found that approximately 30% of low-level clouds are obscured by upper-level clouds, with overlapping cloud occurrence exceeding 90% in tropical regions. Among these, the typical two-layer cloud system composed of upper-level ice clouds and lower-level water clouds is the most prevalent type, accounting for over 50% of overlapping cloud cases (Sourdeval et al., 2016). Therefore, ignoring the vertical complexity of clouds inevitably introduces retrieval biases in cloud microphysical parameters. For instance, Huang et al. (2005) demonstrated using satellite, ground-based microwave radiometer, and lidar observations that the single-layer assumption can lead to a 30% overestimation in COT. Teng et al. (2020) also showed that for ice-over-water cloud systems, retrievals assuming a two-layer structure yield reflectance values more consistent with observations than those based on the single-layer assumption.

Differences in cloud vertical structure can lead to significant discrepancies in the retrieval of cloud properties, thereby affecting the accuracy of simulated radiative effects. In particular, the vertical superposition of liquid and ice clouds raises critical questions: How is the top-of-atmosphere reflectance, as observed by satellites, altered under such configurations? What level of uncertainty is introduced into the retrievals of COT and CER? Furthermore, how does the relationship between COT and CER vary across different vertical cloud structures? To address these questions, COT and CER were retrieved using a bispectral lookup table constructed with the Advanced Radiative Transfer Modeling System (ARMS), driven by FY4A/AGRI (Advanced Geostationary Radiation Imager) observations over central and eastern China from June to August 2018. The retrieved results were subsequently validated using MODIS cloud products. On this basis, we design ten sensitivity experiments with different vertical cloud structures to systematically assess the impact of cloud layering on visible and shortwave infrared reflectance, and to investigate how variations in vertical structure influence the relationship between COT and CER. This work aims to elucidate the uncertainties introduced by vertical cloud structure in satellite-based cloud property retrievals.

This paper is organized as follows: Section 1 outlines the importance and current progress of satellite-based retrievals of COT and CER. Section 2 describes the data sources and retrieval algorithm. Section

https://doi.org/10.5194/egusphere-2025-2939
Preprint. Discussion started: 8 July 2025

3 presents a validation of the retrieval results against MODIS cloud products. Section 4 investigates the sensitivity of simulated reflectance, COT, and CER to different vertical cloud structures using ARMS. Section 5 summarizes the findings and provides discussion.

2 Data，Model and Methods

2.1 FY4A/AGRI Data

The satellite data used in this study consist of FY4A/AGRI Level-1 full-disk observations. The FY4A satellite provides high-frequency measurements of the Earth's atmosphere and surface, delivering critical data and products to improve weather forecasting accuracy. Since March 2018, these data have been available for download from the Fengyun Satellite Remote Sensing Data Service Network (https://satellite.nsmc.org.cn/DataPortal/cn/home/index.html). The AGRI instrument onboard FY4A comprises 14 spectral channels, including six visible and near-infrared bands, two mid-infrared bands, two water vapor bands, and four thermal infrared bands. The AGRI completes a full-disk scan every 15 minutes. The spatial resolution ranges from 0.5 to 1.0 km for visible and near-infrared channels, and from 2 to 4 km for infrared channels. The high spatial and temporal resolution of AGRI is advantageous for identifying and tracking small-scale, rapidly evolving systems such as nascent convection (Yang et al., 2017).

To investigate the impact of different vertical cloud structures on COT and CER, satellite observations from June to August 2018 over central China (105°E~120°E, 24°N~39°N) were selected. The retrieval experiments and validations of COT and CER were performed using two spectral channels: visible (0.55–0.75 μm) and shortwave near-infrared (1.58–1.64 μm).

2.2 ARMS Model

This study employs the Advanced Radiative Transfer Modeling System (ARMS) model developed in China, which utilizes a fast transmittance calculation scheme (Weng et al., 2020). In the simulation process, ARMS takes atmospheric optical parameters as inputs, where the optical thickness varies in response to changes in the atmospheric environment. These parameters are typically generated using spectral libraries containing line-by-line absorption coefficients. Optical properties related to five hydrometeor categories—cloud droplets, rain, cloud ice, graupel, snow, and hail are computed for each atmospheric layer. Liquid hydrometeors are assumed to be spherical, and their scattering parameters are derived using Mie theory. Given an effective particle radius, the total number of particles per layer is

https://doi.org/10.5194/egusphere-2025-2939
Preprint. Discussion started: 8 July 2025

determined from the hydrometeor water content. For ice clouds, scattering by particles with diameters equal to or larger than the radiation wavelength is treated using the T-matrix method (Bi and Yang, 2017), and the results are stored in a scattering database. The accuracy of the ARMS model has been validated in previous studies (Yang et al., 2020; Tang et al., 2021).

In this study, the ARMS radiative transfer model is employed to simulate cloud reflectance across multiple spectral bands. Atmospheric background fields are sourced from the ERA5 reanalysis dataset (Hersbach et al., 2020), which provides vertical profiles of temperature, water vapor, and ozone, along with pressure levels, cloud liquid and ice water content, surface temperature, and surface type. In addition, a series of idealized sensitivity experiments are conducted by constructing different cloud vertical structures, aiming to investigate the impacts of cloud layering on reflectance, cloud optical thickness (COT), and cloud effective radius (CER).

2.3 COT and CER retrieval

The bispectral retrieval algorithm, developed based on the optical and radiative properties of liquid and ice clouds, is one of the most widely used methods for retrieving cloud parameters. It has been extensively applied to a variety of satellite instruments (Platnick et al., 2017; Min et al., 2017; Letu et al., 2018; Zhuge et al., 2021). In this study, the COT and CER are retrieved using observations from the FY4A/AGRI visible channel (0.65 μm) and shortwave near-infrared channel (1.61 μm), with forward simulations provided by the ARMS radiative transfer model. The overall retrieval procedure is illustrated in Fig. 1.

Based on the approach proposed by Zhuge et al. (2017), a fast cloud detection algorithm is implemented using AGRI Level-1 data (0.47, 0.65, 0.825, and 1.61 μm) to distinguish between cloudy pixels and clear-sky conditions, with thresholds listed in Table 1. Pixels with brightness temperatures (10.7 μm) below 233 K are classified as ice clouds, and those above 273 K as liquid clouds. ERA5 reanalysis data are interpolated in time and space to match the spatial and temporal grids of FY4A/AGRI satellite observations. Temporal interpolation is performed linearly between the two nearest ERA5 time steps, while spatial interpolation uses inverse distance weighting based on the four closest ERA5 grids to each satellite pixel. The matched atmospheric profiles, surface conditions, and geometric angles are then input into the ARMS model. The simulated reflectance under specific atmospheric and cloud conditions is utilized to generate look-up tables (LUTs), which support the retrieval of COT and CER for

https://doi.org/10.5194/egusphere-2025-2939
Preprint. Discussion started: 8 July 2025

both liquid and ice phase clouds (Table 2). Fig. 2 illustrates the theoretical relationship between COT and CER for liquid clouds (a) and ice clouds (b) under fixed solar and viewing geometry. It can be seen that, for both cloud types, the reflectance in the visible and shortwave infrared channels generally increases with increasing COT and decreases with increasing CER. This behavior is consistent with previous studies (Letu et al., 2020; Zhuge et al., 2021).

Building upon these physical principles, this study proposes a novel retrieval algorithm for COT and CER, referred to as the DORF (Differential Operator-based Random Forest) algorithm, which integrates multispectral information with spatial structure features. Fig. 3 illustrates the structure and specific schematics of the DORF model. The core of the method is a Random Forest (RF) model that leverages both FY4A/AGRI multispectral observations and spatial gradient features to construct a nonlinear retrieval framework. In this framework, a Random Forest (RF) model is trained using MODIS cloud products as ground truth labels. The input variables include multispectral reflectance and spatial gradient features from FY4A/AGRI, as well as prior estimates of COT and CER from a physically based lookup table generated by the ARMS. During prediction, only FY4A/AGRI data are used, ensuring the model's independence from MODIS and demonstrating its transferability to geostationary satellite observations. While RF has been widely used in environmental parameter estimation (Stafoggia et al., 2019), its applications in cloud remote sensing remain relatively limited. This study demonstrates that, when integrated with physically meaningful spatial and physical features, the RF model can serve as an effective and interpretable method for retrieving cloud microphysical properties from satellite observations.

Specifically, six representative channels from the AGRI (i.e., channels 2, 5, 6, 7, 10, and 12) are selected to characterize the cloud's reflectance, absorption, and emission properties across different spectral bands. For each selected channel R^i (i=1, …,6), we compute the first-order spatial gradients in the horizontal (x) and vertical (y) directions using the Sobel operator, yielding gradient magnitudes:

$$G_i = \sqrt{\left(\partial_x R_i\right)^2 + \left(\partial_y R_i\right)^2} \quad (1)$$

The final input vector for each satellite pixel is then formulated as:

$$x = \left[R_1, R_2, \ldots, R_6, G_1, G_2, \ldots, G_6\right] \in R^{12} \quad (2)$$

Where x denotes the combined spectral and spatial features, serves as input to the RF model. The Sobel operator is applied to each of the six selected AGRI channels using 3×3 convolution kernels to

https://doi.org/10.5194/egusphere-2025-2939
Preprint. Discussion started: 8 July 2025

180 approximate derivatives in the east-west and north-south directions. This magnitude reflects the local edge strength and spatial texture of the cloud field. Combined with the corresponding spectral reflectance values, they form the complete input vector *x* for the RF model. The nonlinear relationship between these features and the target cloud properties (COT and CER) is established using the MODIS official cloud products as the reference dataset.

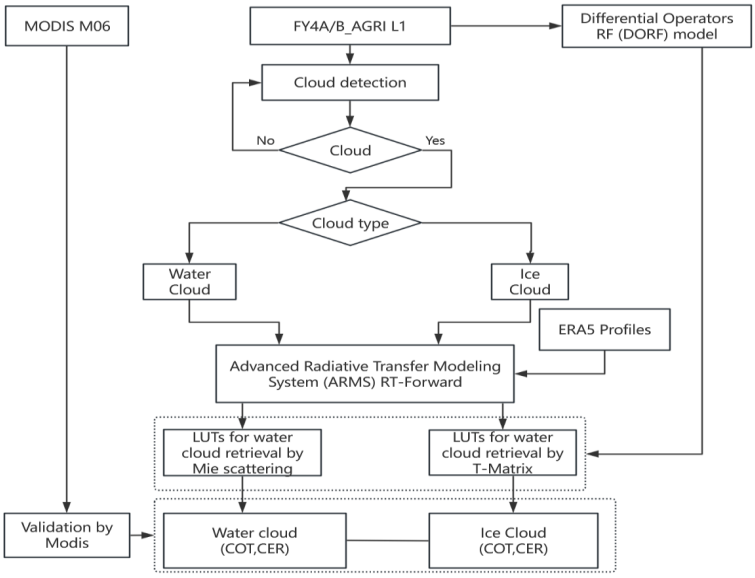

185

Figure 1. Framework of the COT and CER retrieval algorithm for FY4A_AGRI

Table 1. Cloud detection thresholds for FY4A AGRI.

Channel	Physical significance	Threshold
$\frac{T_{0.65}-R_{0.825}}{R_{0.65}+R_{0.825}}$	Normalized Difference Cloud Index (NDCI)	>0.12
$R_{0.65}$	Reflectance	>0.3
$\frac{T_{0.65}-R_{1.61}}{R_{1.61}+R_{0.65}}$	Normalized Difference Snow Index (NDSI)	>0.26
$R_{0.47}$	Reflectance	>0.15

Table 2. Input parameters and grid points of the variables used to build the LUT version of the FY4A_AGRI.

Variables	Range	Number of grids	Unit
Sun zenith	0,5,10,15,20,25,30,35,40,45,50,55,60,65,70,75,80	15	degree
Satellite zenith	0,5,10,15,20,25,30,35,40,45,50,55,60,65,70,75,80	15	-
Relative Azimuth	0,10,20,30,40,50,60,70,80,90,100,110,120,130,140,150,1	19	-

https://doi.org/10.5194/egusphere-2025-2939
Preprint. Discussion started: 8 July 2025

	60,170,180		
Water cloud optical thickness	0.25,0.32,0.4,0.5,0.6,0.8,1.0,1.26,1.58,1.99,2.51,3.16, 3.98,5.01,6.3,7.94,10.0,12.59,15.85,19.95,25.12,31.62, 39.81,50.12,63.1,79.4,100.0,125.9,158.5	27	
Water cloud effective radius	2,4,5,8,11,14,17,20,26,30,36,42,50,60	12	μm
Ice cloud optical thickness	0.25,0.32,0.4,0.5,0.6,0.8,1.0,1.26,1.58,1.99,2.51,3.16, 3.98,5.01,6.3,7.94,10.0,12.59,15.85,19.95,25.12,31.62, 39.81,50.12,63.1,79.4,100.0,125.9,158.5	27	
Ice cloud effective radius	5,10,15,25,30,35,40,50,60,70,80,90,110,130	12	μm

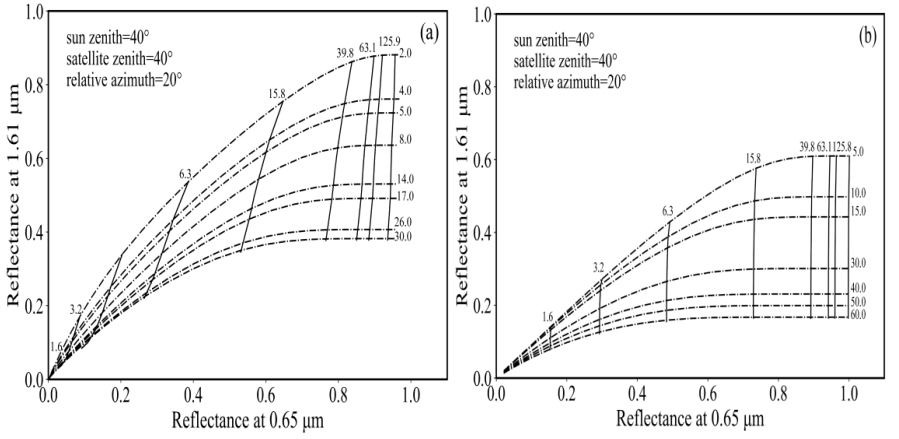

Figure 2. Bispectral reflectance LUTs of cloud reflectance at 0.65 um and 1.61 um for water(a) and ice(b) phases when the solar zenith angle is 40°, the sensor viewing zenith angle is 40°, and the relative azimuth angle is 20°, and the underlying surface is land. The dashed line represents the CER, and the solid line represents the COT.

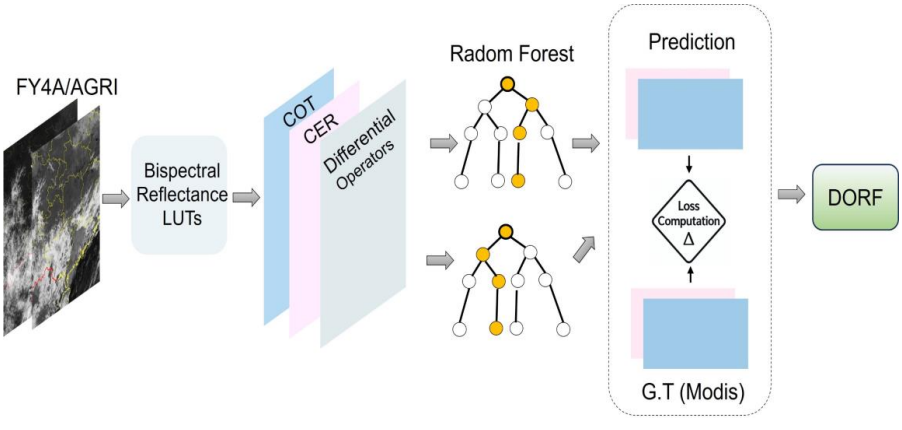

Figure 3. Schematic of the DORF model for COT and CER prediction based on FY-4A/AGRI observations.

3 COT and CER Retrievals and Comparisons

In the retrieval process, COT and CER are treated as independent variables derived from different

https://doi.org/10.5194/egusphere-2025-2939
Preprint. Discussion started: 8 July 2025

spectral bands, though they are physically coupled. COT reflects the vertical integration of cloud water content, while CER represents average particle size affecting scattering efficiency. Together, they determine cloud radiative properties and are linked through the cloud water path.

3.1 Overall Performance

The COT and CER products retrieved from MODIS remain among the most reliable satellite-derived cloud parameters, offering long-term time series with high accuracy and stability (Platnick et al., 2003; 2017). To evaluate the accuracy of cloud property retrievals from FY4A/AGRI, a comparative analysis was conducted against the MODIS Collection 6.1 MOD06 cloud product for daytime data spanning from June 1 to August 31, 2018. Fig. 4 presents scatterplots of CER and COT comparisons over eastern and central China (105~120°E, 24~39°N). The CER values retrieved from FY4A/AGRI show strong agreement with those from MODIS MOD06, with a coefficient of determination (R^2) of 0.91, a mean absolute error (MAE) of 2.0 μm, and a root-mean-square error (RMSE) of 3.36 μm. Similarly, the FY4A/AGRI-derived COT exhibits good consistency with MODIS MOD06, with R^2, MAE, and RMSE values of 0.87, 3.9, and 8.03, respectively.

Probability density distributions of CER and COT from both sensors further support these findings (Fig. 5). For CER < 13 μm, FY4A/AGRI tends to underestimate CER relative to MODIS, whereas in the range of 14~23 μm, FY4A/AGRI generally retrieves larger CER values than MODIS. As CER increases further, the differences between the two sensors diminish. A similar trend is observed in COT retrievals: MODIS yields higher COT values than FY4A/AGRI when COT < 10, while the opposite is true for higher COT values. These patterns suggest that FY4A/AGRI is less sensitive to optically thin clouds compared to MODIS, but still demonstrates robust detection and retrieval capabilities for more extensive cloud systems (Min et al., 2017).

https://doi.org/10.5194/egusphere-2025-2939
Preprint. Discussion started: 8 July 2025

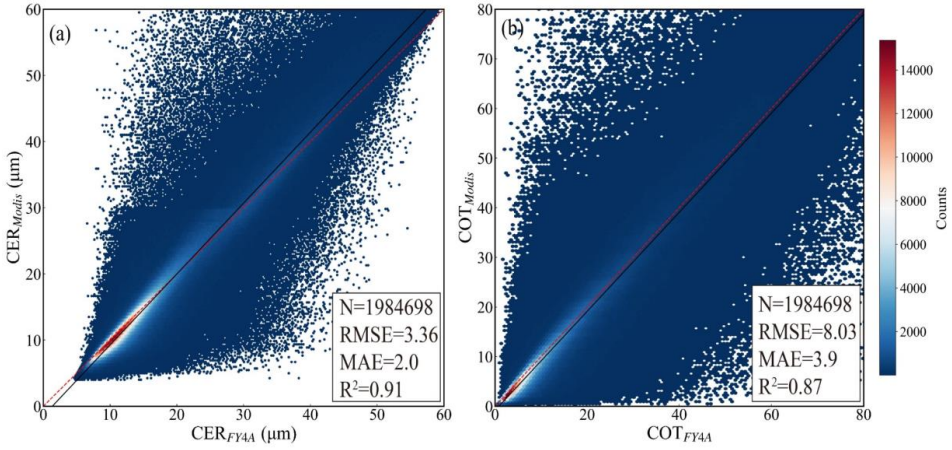

Figure 4. Scattering plot (a and b) of COT and CER from MODIS C6 (MOD06) and FY4A/AGRI data in the selected area.

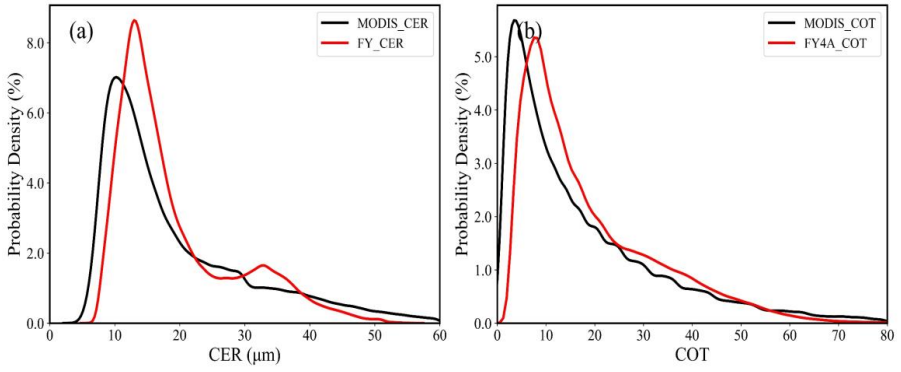

Figure 5. Probability density function (PDF) of the FY4A/AGRI retrieval results and the MODIS cloud products in the region. The red and black solid line shows the FY4A/AGRI results and the MODIS results, respectively.

3.2 Case Study

To further verify the reliability of the ARMS model and the retrieval algorithm, a case study was conducted using a mesoscale convective system (MCS) that occurred over central-eastern China on August 2, 2018, and persisted for approximately 17 hours. The spatial distributions of COT and CER retrieved from FY4A/AGRI were compared with MODIS cloud products for validation.

At 04:00 UTC on August 2, 2018, the FY4A/AGRI false-color imagery revealed two isolated convective cloud systems moving northward in parallel (Fig. 6a). Fig. 6b shows that the region north of 30°N was predominantly covered by high-altitude ice clouds, while the area below was mainly composed of low-level water clouds. Fig. 6c and 6d present the retrieved COT distributions from FY4A/AGRI and

https://doi.org/10.5194/egusphere-2025-2939
Preprint. Discussion started: 8 July 2025

Terra MODIS (Cloud_Optical_Thickness_16), respectively. Two distinct high-value COT centers (>65) are evident in the region spanning 31~32.5°N and 111~113°E. Quantitatively, the COT values retrieved by FY4A/AGRI in the high-value regions closely match those from MODIS. However, in the low-COT areas, FY4A/AGRI tends to overestimate values by approximately 12% compared to MODIS. This deviation differs from the findings of Chen et al. (2020), who reported that FY4A/AGRI underestimated COT by about 10% in high-value regions during a retrieval over the Wuhan area. The discrepancy may stem from differences in the parameterization of ice-phase particles in the radiative transfer models used for retrieval.

In terms of CER retrievals, FY4A/AGRI and MODIS (Cloud_Effective_Radius_16) exhibit similar spatial distribution patterns. When CER values exceed 30 μm, the retrievals from both sensors are generally consistent, especially within the two high-value centers of ice clouds located between 31~32.5°N and 111~113°E, where their retrievals closely match (Fig. 6e-f). However, to the north of these two centers (32~34°N), MODIS reveals several localized regions with CER values exceeding 50 μm, whereas the corresponding CER values from FY4A/AGRI range between 40–50 μm. Additionally, in some thin water cloud regions, MODIS retrievals primarily show CER values between 20~30 μm, while FY4A/AGRI reports lower values concentrated between 10~20 μm.

These differences can be attributed mainly to two factors: (1) Spatial resolution differences between the sensors. MODIS provides cloud products at a horizontal resolution of 1 km, allowing for finer detection of clear-sky boundaries and thin or broken cloud structures (Maddus et al., 2010). FY4A/AGRI has a coarser resolution of 4 km, which inevitably leads to a loss of small-scale cloud details; (2) Cloud horizontal inhomogeneity within the FY4A/AGRI pixels. Therefore, in this case study, MODIS demonstrates a more detailed retrieval of fragmented cloud regions near ice clouds compared to FY4A/AGRI.

https://doi.org/10.5194/egusphere-2025-2939
Preprint. Discussion started: 8 July 2025

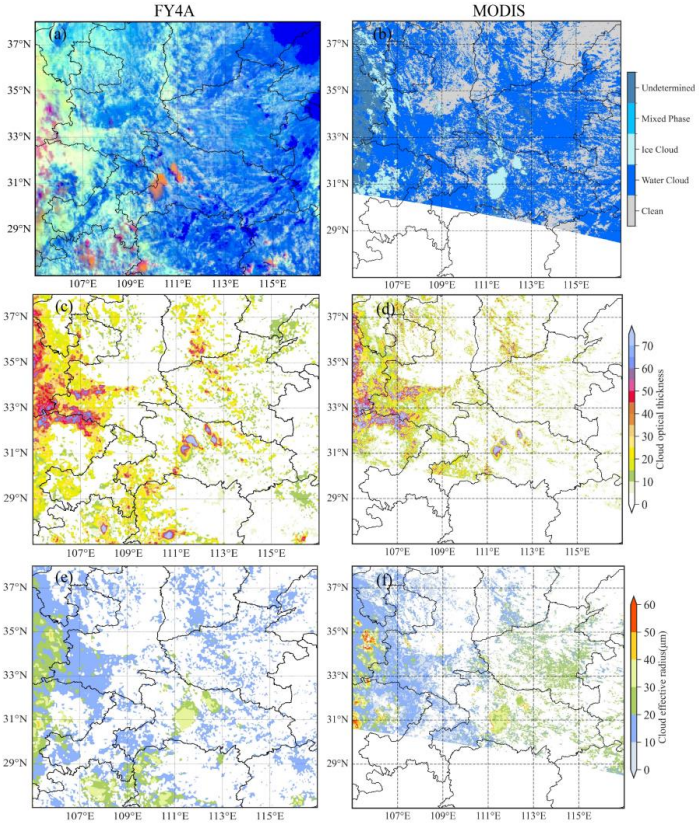

Figure 6. Comparison of retrieved optical parameters using the FY-4 AGRI with MODIS cloud products (Cloud_Optical_Thickness_16 and Cloud_Effective_Radius_16). The observation time of the FY-4 AGRI is 04:00 UTC on 2 August 2018 and the MODIS observation time is 03:35 UTC. (a) False-color image (red, 0.65 μm; green, 1.61 μm; blue, 10.7 μm reversed) where thick ice clouds are orange colored, and low clouds are white colored. (b, d, f) cloud-top phase, COT(unitless), CER(unit: μm) from Collection-6.1 MOD06 at 0335 UTC August 2, 2018. (c,e) COT(unitless), CER(unit: μm) derived FY4A/AGRI at 0400 UTC August 2, 2018.

4 Cloud Microphysical and Radiation Response to Cloud Vertical Structure

Cloud vertical structure includes the number of cloud layers, cloud top height, cloud base height, cloud thickness, cloud fraction, and the vertical distribution of cloud microphysical properties. It reflects the thermodynamic, dynamic, and microphysical processes within the cloud system and plays an important role in weather and climate (Xu et al., 2023). To quantitatively investigate the effects of cloud layer number and cloud phase on cloud reflectance, COT and CER, this study builds upon the case study retrieval results from Section 3.2. Cloud water profiles are categorized into single-layer, double-layer, and triple-layer clouds, and by adjusting the cloud liquid/ice water content in each layer, the sensitivity of cloud reflectance, COT and CER under different vertical cloud structure conditions is systematically

https://doi.org/10.5194/egusphere-2025-2939
Preprint. Discussion started: 8 July 2025

analyzed.

4.1 Cloud water/ice content Profiles Classification

To investigate the impact of cloud vertical structure on COT and CER, 221 vertical profiles of cloud liquid and ice water content were extracted from ERA5 at 04:00 UTC on 2 August 2018 over the region 110~114°E and 30~33°N (Section 3.2). Based on empirical rules, each profile was classified into different structural types. The number of peaks in liquid/ice water content was used to determine the number of cloud layers, while cloud phase was inferred by pressure level: ice clouds above 450 hPa, and liquid clouds below 700 hPa and between 700–450 hPa.

Specifically, single-layer clouds, characterized by one peak, were divided into three types: high-level ice clouds, mid-level water clouds, and low-level water clouds. Two-layer cloud structures, identified by two peaks, were further categorized into five subtypes based on the cloud phase (ice or water) and the relative liquid or ice water content in the upper, middle, and lower layers. Three-layer profiles, indicated by three peaks, generally represent a typical ice–water–water cloud configuration (Fig. 7).

Statistical results (Table 3) show that single-layer clouds account for 48% of the profiles, two-layer clouds 46%, and three-layer clouds 6%. These proportions are consistent with the findings of Xu et al. (2023), who reported that single-layer clouds dominate (55.4%) in radiosonde observations, with two-layer systems being the most frequent among multilayer clouds. This agreement supports the validity and physical relevance of the classification method used.

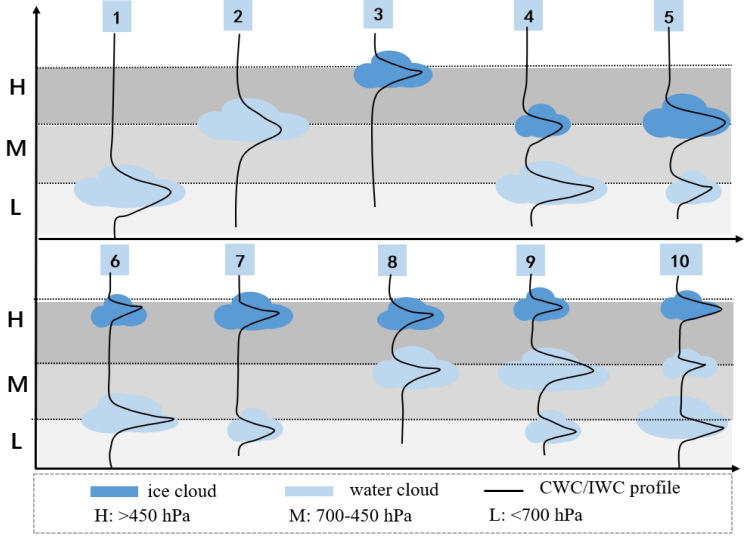

https://doi.org/10.5194/egusphere-2025-2939
Preprint. Discussion started: 8 July 2025

Figure 7. Vertical structure types of cloud water and ice content profiles from ERA5. The "large cloud" profiles correspond to the original profiles with a fivefold increase in cloud water or ice content, while the "small cloud" profiles represent the unmodified original profiles. The distinction between large and small clouds is not explicitly marked in the figure but can be inferred from the differences in water content.

Table 3 Proportions of single-layer, two-layer, and three-layer Cloud Profiles and Corresponding Mode Classifications

Cloud Layers	Height	Cloud type	Exp No.	Ratio
Single Layers Cloud	H	Ice	3	
	M	Water	2	48%
	L	Water	1	
Two-layer Clouds	H+M	Ice + Water	8	46%
	H+L	Ice + Water	6,7	
	L+M	Ice + Water	4,5	
Three-layer Clouds	H+M+L	Ice + Water +Water	9,10	6%

4.2 Sensitivity of Reflectance to Cloud Vertical Structure

Based on the classification, Fig. 8 shows the sensitivity of cloud reflectance to CER variations for three single-layer cloud types under increased LWC or IWC. For low-level water clouds, channel 2 reflectance rises from 0.6 to 0.7 as CER increases from 2 to 10 μm, while channel 5 first decreases then rise to 0.68 (Fig. 8a). Increasing LWC enhances channel 2 reflectance by about 0.1, with a smaller effect on channel 5. Mid-level water clouds exhibit significant reflectance changes in channel 2 only when CER exceeds 10 μm, stabilizing beyond 25 μm (Fig. 8b). High-level ice clouds show slightly higher reflectance in both channels compared to water clouds (Fig. 8c). Overall, increased LWC in low-level clouds notably boosts reflectance, especially in the visible channel, by approximately 15% more than mid- or high-level clouds.

Fig. 9 illustrates reflectance changes for two-layer cloud structures. When lower-layer LWC increases and upper-layer COT is low, reflectance in channels 2 and 5 increases minimally due to incomplete masking (Fig. 9a). For mid-level ice over low-level water clouds, channel 2 and 5 reflectance decrease markedly, with channel 5 more strongly attenuated (Fig. 9b). Increasing mid-level LWC mainly enhances

https://doi.org/10.5194/egusphere-2025-2939
Preprint. Discussion started: 8 July 2025

reflectance for CER < 10 μm, indicating high sensitivity of small particles (Fig. 9c). A similar pattern is seen with increased high-level IWC, though channel 2 reflectance decreases and channel 5 increases at CER > 50 μm (Fig. 9d). The combination of high-level ice over low-level water yields the highest reflectance among two-layer clouds (Fig. 9e). When water clouds lie at mid-level, added upper-level IWC raises reflectance at CER = 30 μm by up to 23% in both channels (Fig. 9f).

Three-layer clouds display more complex nonlinear reflectance behavior (Fig. 10). Increasing LWC in lower or middle layers causes alternating enhancement or reduction of reflectance across CER ranges (Fig. 10a). With higher upper-level IWC, channels 2 and 5 show pronounced increases at CER = 10 μm and > 50 μm (Fig. 10b), reflecting strong shortwave scattering by large ice crystals and partial penetration effects on lower layers. These observations align with Li et al. (2011), who found that multilayer clouds have weaker shortwave reflectance than single-layer clouds due to their higher cloud tops allowing shortwave radiation to partially transmit to lower clouds or the surface.

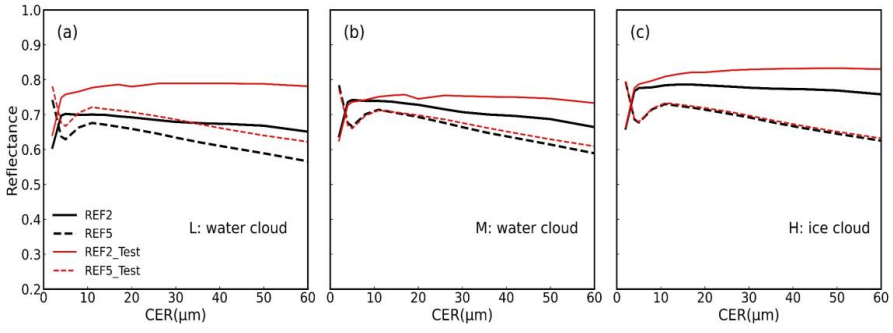

Figure 8. Variation of cloud reflectance at Channel 2 (solid lines) and Channel 5 (dashed lines) with cloud effective radius (CER) under different LWC or IWC condition. Black lines correspond to reflectance simulated using the original LWC/IWC profiles from ERA5 reanalysis, while red lines represent reflectance simulated with LWC/IWC increased by a factor of 5. Three single-layer cloud types are shown: low-level water clouds (a, Exp 1), mid-level water clouds (b, Exp 2), and high-level ice clouds (c, Exp 3). The simulations assume a solar zenith angle of 40°, sensor viewing zenith angle of 40°, and relative azimuth angle of 20°.

https://doi.org/10.5194/egusphere-2025-2939
Preprint. Discussion started: 8 July 2025

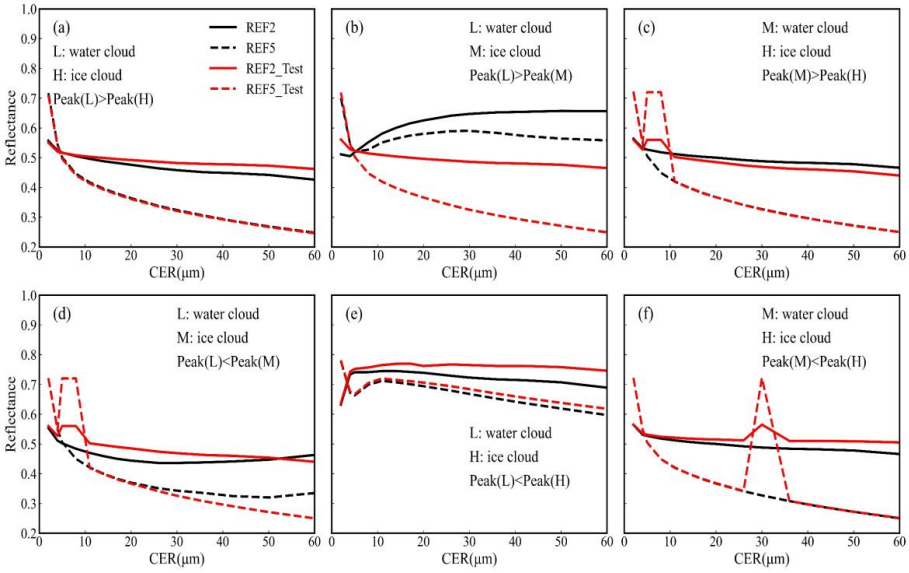

Fig. 9. Reflectance–CER Relationships under varying LWC/IWC Conditions for Six Overlapping cloud types. (a) Low-level water cloud with increased LWC beneath high-level ice cloud (Exp 6); (b) Low-level water cloud with increased LWC beneath mid-level ice cloud (Exp 4); (c) Mid-level water cloud with increased LWC beneath high-level ice cloud (Exp 8); (d) Low-level water cloud with increased LWC overlain by high-level ice cloud (Exp 7); (e) Low-level water cloud with increased IWC beneath mid-level ice cloud (Exp 5); (f) Mid-level water cloud with increased IWC beneath high-level ice cloud (Exp 8).

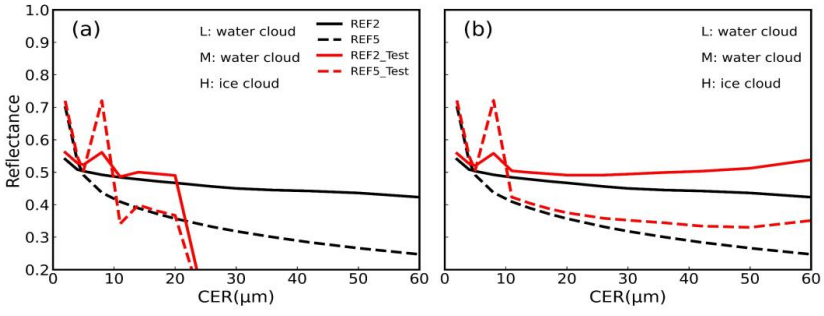

Figure10. Similar to Fig. 9, but for multi-layer clouds (a) Exp 9 and (b) Exp 10.

4.3 Sensitivity of COT–CER Relationship to Cloud Vertical Structure

To investigate the impact of vertical cloud structure perturbations on the retrieval of cloud optical thickness (COT) and cloud effective radius (CER), representative configurations of single-layer, two-layer, and three-layer clouds were selected (Fig. 11). By perturbing LWC or IWC at specific vertical levels and comparing the results with unperturbed cases, the change in optical thickness (ΔCOT) was

https://doi.org/10.5194/egusphere-2025-2939
Preprint. Discussion started: 8 July 2025

quantified.

Fig. 11a and 10b show ΔCOT as a function of CER after increasing the LWC in low- and mid-level water clouds, respectively. For single-layer clouds, ΔCOT increases nonlinearly with CER, showing a rapid rise when CER is below 15 μm before approaching saturation. Notably, when CER < 10 μm, increasing LWC in mid-level water clouds leads to a maximum ΔCOT of 52, which is approximately 1.6 times greater than that resulting from the same perturbation in low-level clouds. This indicates that mid-level clouds exhibit a stronger optical response to LWC perturbations under small particle size conditions.

For two-layer structures, three typical modes were analyzed: (1) mid-level ice cloud over low-level water cloud (Fig. 11c), (2) high-level ice cloud over low-level water cloud (Fig. 11d), and (3) high-level ice cloud over mid-level water cloud (Fig. 11e). In all cases, ΔCOT changes from LWC/IWC perturbations were generally smaller than in single-layer clouds, especially for CER < 20 μm, the mean COT increase due to low- and mid-level water cloud variations in single-layer clouds exceeds that in double-layer clouds by about 24%, primarily due to the masking effect of upper-level ice clouds in double-layer structures. Specifically, for mid-level ice over low-level water clouds, increasing low-level LWC caused negative ΔCOT values (down to –8) at CER < 10 μm, while increasing mid-level ice IWC led to positive ΔCOT up to 12, indicating that overlying ice clouds can reduce the optical impact of underlying water clouds at small particle sizes. In contrast, the high-level ice cloud over low-level water cloud configuration exhibited a strong positive ΔCOT response to increases in LWC. For the high-level ice cloud over mid-level water cloud scenario, increasing mid-level LWC induced a non-monotonic ΔCOT variation at CER values below 10 μm, initially increasing and then decreasing, likely due to complex radiative interactions between the cloud layers.

For three-layer clouds (Fig. 11f), increases in mid- or lower-level LWC significantly enhance ΔCOT, although peak values are slightly lower than those observed in single-layer and mid-level clouds. Compared to increases in IWC, LWC increases in the lower water cloud induce larger ΔCOT changes, especially at small CER where shortwave reflectance is strongest. Furthermore, we find that the sensitivity patterns of LWC/IWC perturbations are consistent across single-, two-, and three-layer cloud structures, and the largest COT variations occur at CER values less than 20 μm, with this influence gradually diminishing as CER increases.

https://doi.org/10.5194/egusphere-2025-2939
Preprint. Discussion started: 8 July 2025

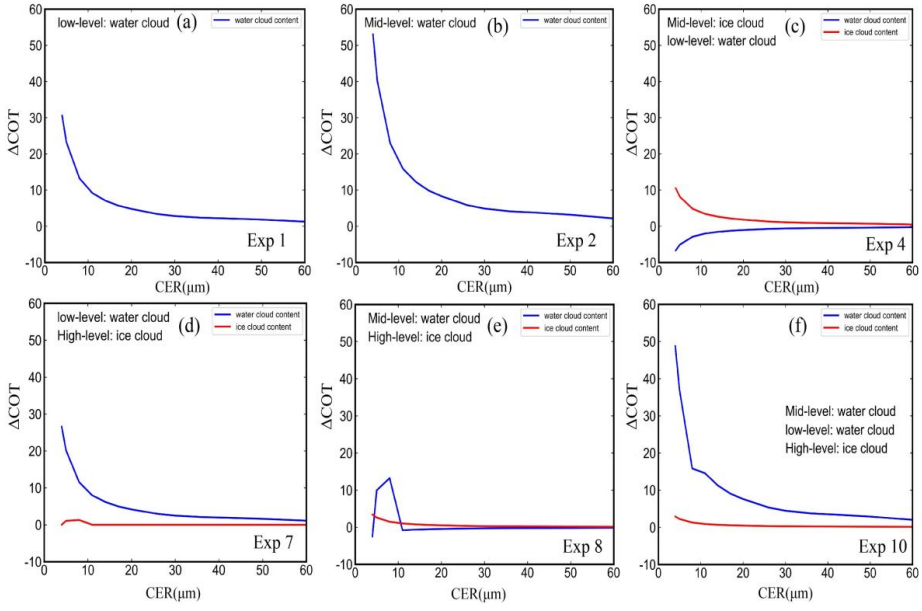

Figure 11. Changes in cloud optical thickness (ΔCOT) as a function of CER for six selected vertical cloud structure types (Exp 1, 2, 7, 8, and 10). Each panel shows the ΔCOT resulting from adding LWC or IWC to a specific vertical layer relative to a reference state without that layer. Blue lines represent the contribution of added LWC, while red lines represent added IWC. Model numbers are indicated in each panel. when the solar zenith angle is 40°, the sensor viewing zenith angle is 40°, and the relative azimuth angle is 20°.

5 Conclusions

Based on FY4A/AGRI geostationary satellite observations over eastern and central China during June–August 2018, this study developed a bispectral retrieval algorithm for cloud optical thickness (COT) and cloud effective radius (CER), employing the Advanced Radiative Transfer Modeling System (ARMS). The algorithm's reliability was validated against MODIS cloud products. Additionally, ten idealized vertical cloud structures were constructed to systematically evaluate the sensitivity of visible and shortwave-infrared reflectance to cloud layer variations. The associated changes in retrieved COT and CER highlight the significant uncertainties introduced by vertical cloud heterogeneity in microphysical retrievals.

The COT and CER retrieved from FY4A/AGRI show good agreement with MODIS, with correlation coefficients of 0.87 and 0.91, respectively, indicating reliable performance in capturing cloud microphysical properties. A case study reveals that FY4A/AGRI performs well in high-COT regions but tends to overestimate COT in low-value areas. CER retrievals are generally consistent with MODIS in

https://doi.org/10.5194/egusphere-2025-2939
Preprint. Discussion started: 8 July 2025

ice cloud regions, though underestimations occur in thin water clouds. Due to resolution differences, FY4A/AGRI performs well in large-scale cloud retrievals but has lower capability than MODIS in representing thin and small-scale clouds.

To better illustrate the radiative impacts of cloud vertical structure and their implications for COT and CER retrievals, a conceptual schematic is presented in Fig. 12. It visualizes how different configurations of cloud layers affect the observed reflectance and retrieval accuracy from geostationary satellite sensors. The study shows that cloud reflectance sensitivity in visible and near-infrared channels varies significantly with vertical cloud structure. For single-layer liquid clouds, increasing low-level LWC strongly enhances reflectance, with visible channel increases about 15% greater than those for mid-level liquid or high-level ice clouds. In two-layer clouds with mid-level liquid and high-level ice, increasing mid-level LWC mainly boosts reflectance in small particle size regions (CER < 10 μm). In three-layer systems, reflectance dependence on CER is more influenced by cloud layer altitude and peak LWC/IWC locations.

Building on the reflectance sensitivity findings, the study further examines how vertical structure perturbations affect the relationship between COT and CER. Increasing LWC/IWC at specific altitudes revealed that ΔCOT exhibits a nonlinear trend with CER in single-layer clouds, with mid-level LWC increases causing up to 1.6 times the ΔCOT of low-level increases. Among various cloud structures, the most significant increase in COT occurs at smaller CER values (<15 μm) when LWC increases in the low to mid-level water clouds, while variations in high-level IWC contribute minimally to COT changes. These findings highlight the critical role of low-level water cloud variability on shortwave radiation reflection and optical thickness in both modeling and retrieval processes.

These results suggest that assuming a single homogeneous cloud layer in remote sensing retrievals can cause significant errors. Upper-level ice clouds can shield lower-level water clouds, leading to underestimated total reflectance and systematic low bias in COT. CER retrievals are also sensitive to cloud layer height and water/ice content distribution, with neglect of inter-layer radiative effects increasing uncertainty. Sensitivity experiments indicate that for CER < 20 μm, the mean increase in COT caused by variations in single-layer clouds exceeds that in double-layer cloud structures by approximately 24%. Incorporating prior cloud vertical structure information from active sensors or reanalysis can improve COT and CER retrieval accuracy, as well as enhancing the monitoring and forecasting of severe convective weather.

https://doi.org/10.5194/egusphere-2025-2939
Preprint. Discussion started: 8 July 2025

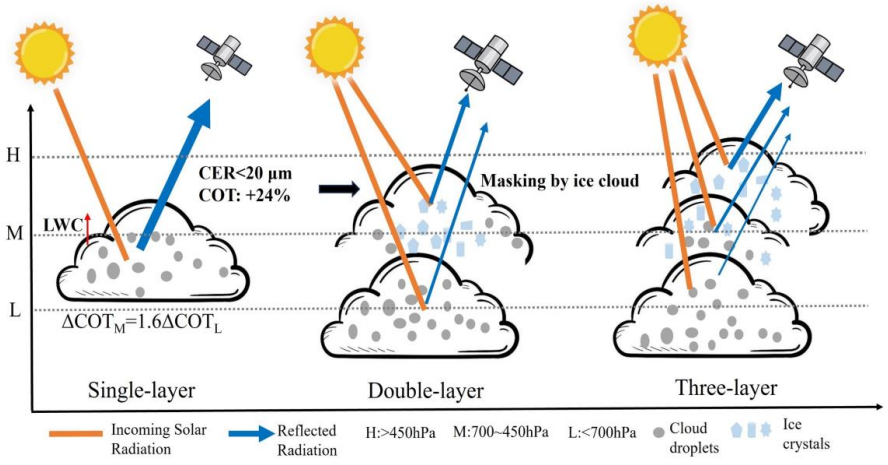

Fig. 12. Conceptual diagram illustrating the radiative characteristics and retrieval implications of COT and CER under different vertical cloud structures.

Code availability. The code used in this study are available from the corresponding author upon reasonable request(ghlyy@mail.iap.ac.cn).

Data availability. The FY4A/AGRI data used for the main COT and CER retrieval in this study are released from the Fengyun Meteorological Satellite Remote Sensing Data Service Platform (https://satellite.nsmc.org.cn/DataPortal/cn/data/order.html). The MODIS cloud product used for the DORF model building and for validating the spatial distributions of retrieved COT and CER from FY4A/AGRI(https://ladsweb.modaps.eosdis.nasa.gov/search/order/1/MOD06_L2--61,MYD06_L2--61). The ERA5 reanalysis datasets are used to provide atmospheric temperature, humidity, and pressure profiles as input to the ARMS radiative transfer model (Hersbach et al., 2020). Additionally, vertical profiles of cloud liquid water and ice water content from ERA5 are used to construct and classify the idealized cloud vertical structure models used in the sensitivity experiments (https://cds.climate.copernicus.eu/datasets/). The Advanced Radiative Transfer Modeling System (ARMS) model developed in China (Weng et al., 2020), and the package is available from hanyang@cma.gov.cn. The random forest technique is available at https://scikit-learn.org/stable/modules/generated/sklearn.ensemble.

Author contributions. JS conceptualized the study, and wrote the original draft. JS and YL designed the algorithms, and revised the manuscript. HH, QL, and CY validated results and supervised the research. YS and ZC performed the simulations.

Competing interests. The authors declare that they have no known competing financial interests or personal relationships that could have appeared to influence the work reported in this paper.

Acknowledgements. The authors would like to thank the National Satellite Meteorological Center for providing the FY4A/AGRI Level-1 full-disk observation data, the National Aeronautics and Space

https://doi.org/10.5194/egusphere-2025-2939
Preprint. Discussion started: 8 July 2025

Administration (NASA) Level-1 and Atmosphere Archive &Distribution System (LAADS) for providing the MODIS cloud products, the European Centre for Medium-Range Weather Forecasts (ECMWF) for the ERA5 reanalysis data. We also acknowledge the Numerical Weather Prediction Center of the China Meteorological Administration (CMA) for the development of the Advanced Radiative Transfer Modeling System (ARMS).

Financial support. This work was jointly supported by the Hunan Provincial Natural Science Foundation of China (grant number 2021JC0009), the National Natural Science Foundation of China (grant number U2242201), and the Hubei Provincial Natural Science Foundation of China (2025AFD423).

References

Bi, L. and Yang, P.: Improved ice particle optical property simulations in the ultraviolet to far-infrared regime. J. Quant. Spectrosc. Radiat. Transf. 189, 228−237, https://doi.org/10.1016/j.jqsrt.2016.12.007, 2017.

Chen, Y., Weng, F., Han, Y., and Liu, Q.: Validation of the community radiative transfer model by using CloudSat data. J. Geophys. Res. Atmos. 113(D8), 114, https://doi.org/10.1029/2007JD009561, 2008.

Chen, Y., Chen, G., Cui, C., Zhang, A., Wan, R., Zhou, S., Wang, D., and Fu, Y.: Retrieval of the vertical evolution of the cloud effective radius from the Chinese FY-4(Feng Yun 4) next-generation geostationary satellites. Atmos. Chem. Phys. 20,1131-1145, https://doi.org/10.5194/acp-20-1131-2020, 2020.

Fang, L., Li, Y., Sun, G., Gao, C., and Lu, Z.: Horizontal and vertical distributions of clouds of different types based on CloudSat–CALIPSO data. Clim. Environ. Res. 21 (5): 547−556. https://doi:10.3878/j.issn.1006-9585.2016.15240, 2016.

George, G., Sarangi, C., Tripathi, S. N., Chakraborty, T., and Turner, A.: Vertical Structure and Radiative Forcing of Monsoon Clouds Over Kanpur During the 2016 INCOMPASS Field Campaign, J. Geophys. Res.-Atmos. 123, 2152–2174, https://doi.org/10.1002/2017JD027759, 2018.

Hersbach, H., Bell，B., Berrisford，P., Hirahara，S., and Thépaut, J.: The ERA5 global reanalysis. Q. J. R. Meteorol. Soc. 146, 1999–2049, https://doi.org/10.1002/qj.3803, 2020.

IPCC., Climate Change 2021. The Physical Science Basis. Contribution of Working Group I to the Sixth Assessment Report of the Intergovernmental Panel on Climate Change, Cambridge, United Kingdom and New York, NY, USA, Cambridge University Press.2021.

Lee, Y., Titov, D., Ignatiev, N., Tellmann, S., Patzold, M., Piccioni, G.: The radiative forcing variability caused by the changes of the upper cloud vertical structure in the Venus mesosphere, Planet. Space Sci. 113, 298–308, https://doi.org/10.1016/j.pss.2014.12.006, 2015.

Letu, H., Nagao, T., Nakajima, T. , Riedi, J., Ishimoto, H., and Baran, A. J.: Ice cloud properties from Himawari-8/AHI next-generation geostationary satellite: Capability of the AHI to monitor the DC cloud generation process. IEEE Trans. Geos. Remote. Sen. 57(6), 1-11, https://doi.org/10.1109/TGRS.2018.2882803, 2018.

Li, J., Yi, Y. H., Minnis, P., Huang, J., Yan, H., Ma, Y., Wang, W., and Ayers, J.: Radiative effect differences between multi-layered and single-layer clouds derived from CERES, CALIPSO, and CloudSat data. J. Quant. Spectrosc. Radiat. Transf. 112(2), 361-375, https://doi.org/10.1016/j.jqsrt.2010.10.006, 2011.

Liu, C., Song, Y. X., Zhou, G. N., Teng, S. W., Li, B., Xu, N., Lu, F., and Zhang, P.: A cloud optical and

https://doi.org/10.5194/egusphere-2025-2939
Preprint. Discussion started: 8 July 2025

microphysical property product for the advanced geosynchronous radiation imager onboard China's Fengyun-4 satellites: The first version. Atmos. Ocean. Sci. Lett. 16, 100337-100343, https://doi.org/10.1016/j.aosl.2023.100337, 2023.

Maddux, B., Ackerman, S., and Platnick, S.: Viewing Geometry Dependencies in MODIS Cloud Products, J. Atmos. Ocean. Tech. 27, 1519–1528, https://doi.org/10.1175/2010JTECHA1432.1, 2010.

Matus, A., and L'Ecuyer, T.: The role of cloud phase in Earth's radiation budget. J. Geophys.Res.Atmos.122, 2559–2578, https://doi.org/10.1002/2016JD025951, 2017.

Min, M, Wu, C., Li, C., Liu, H., Xu, N., Wu, X., Chen, L., Wang, F., Sun, F., Qin, D., Wang, X., Li, B., Zheng, Z., Cao, G., and Dong, L.: Developing the Science Product Algorithm Testbed for Chinese Next-Generation Geostationary Meteorological Satellites: Fengyun-4 Series. J. Meteor. Res. 31, 708-719, https://doi.org/10.1007/s13351-017-6161-z, 2017.

Nakajima, T., and King, M.: Determination of the optical thickness and effective particle radius of clouds from reflected solar radiation measurements. Part I: Theory. J. Atmos. Sci. 47, 1878-1983, https://doi.org/10.1175/1520-0469(1990)047<1878:DOTOTA>2.0.CO;2, 1990.

Platnick, S., King, M., Ackerman, S., Menzel, W., Baum, B., Riédi, J., and Fery, R.: The MODIS cloud products: algorithms and examples from Terra. IEEE Trans. Geosci. Remote. Sens. 41 (2), 459–473, https://doi.org/10.1109/TGRS.2002.808301, 2003.

Platnick, S., Meyer, K. G., King, M.D., Wind, G., Amarasinghe, N., Marchant, B., Yang, P., Ridgway, W., Riedi, J.: The MODIS cloud optical and microphysical products: Collection 6 updates and examples from Terra and Aqua. IEEE Trans. Geosci. Remote. Sens. 55 (1), 502–525. https://doi.org/10.1109/TGRS.2016.2610522, 2017.

Saunders, R., Hocking, J., Turner, E., Rayer, P., Rundle, D., Brunel, P., Vidot, J., Roquet, P., Matricardi, M., Geer, A., Bormann, N., and Lupu, C.: An update on the RTTOV fast radiative transfer model. Geosci. Model. Dev., 11(7): 2717-2737, https://doi.org/10.5194/gmd-11-2717-2018, 2018.

Sourdeval, O., Laurent, C-L., Baran, A. J., and Gérard, B.: A methodology for simultaneous retrieval of ice and liquid water cloud properties. Part 2: Near-global retrievals and evaluation against A-Train products. Q. J. R. Meteorol. Soc. 142(701): 3063-3081, https://doi.org/10.1002/qj.2405, 2016.

Stafoggia, M., Bellander, T., Bucci, S., Davoli, M., de Hoogh, K., de' Donato, F., Gariazzo, C，Lyapustin, A., Michelozzi, P., and Renzi, M.: Estimation of daily PM10 and PM2.5 concentrations in Italy, 2013–2015, using a spatiotemporal land-use random-forest model. Environ. Int. 124, 170–179, https://doi.org/10.1016/j.envint.2019.01.016, 2019.

Suzuki, K., Nakajima, T. Y., Stephens, G. L.: Particle growth and drop collection efficiency of warm clouds as inferred from joint CloudSat and MODIS observations. J. Atmos. Sci. 67 (9), 3019–3032, https://doi.org/10.1175/2010JAS3463.1, 2010.

Tang, F., Zhuge, X., Zeng, M., Li, X., Dong, P., and Han, Y.: Applications of the Advanced Radiative Transfer Modeling System (ARMS) to Characterize the Performance of Fengyun–4A/AGRI. Remote. Sens.13, 3120-3143, https://doi.org/10.3390/rs13163120, 2021.

Teng, S., Liu, C., Zhang, Z., Wang, Y., Sohn, B.-J., and Yung, Y. L.: Retrieval of ice-over-water cloud microphysical and optical properties using passive radiometers. Geophys. Res. Lett. 47, e2020GL088941, https://doi.org/10.1029/2020GL088941, 2020.

Walker, J., MacKenzie, W., Mecikalski, J., and Jewett, C.: An Enhanced Geostationary Satellite–Based Convective Initiation Algorithm for 0–2-h Nowcasting with Object Tracking. J. Appl. Meteorol. Climatol. 51(11), 1931-1949, https://doi.org/https://doi.org/10.1175/JAMC-D-11-0246.1, 2012.

https://doi.org/10.5194/egusphere-2025-2939
Preprint. Discussion started: 8 July 2025

Wang, J., Liu, C., Min, M., Hu, X., Lu, Q., and Letu, H.: Effects and applications of satellite radiometer 2.25-μm channel on cloud property retrievals. IEEE Trans. Geos. Remote. Sen. 56 (9), 5207–5216, https://doi:10.1109/tgrs.2018.2812082, 2018.

Weng, F., Yu, X., Duan, Y., Yang, J., Wang, J.: Advanced radiative transfer modeling system (ARMS): A new-generation satellite observation operator developed for numerical weather prediction and remote sensing applications. Adv. Atmos. Sci. 37, 131−136, https://doi. org/10.1007/s00376-019-9170-2, 2020.

Xu, H., Guo, J., Tong, B., Zhang, J., Chen, T., Guo, X., Zhang, J., and Chen, W.: Characterizing the near-global cloud vertical structures over land using high-resolution radiosonde measurements. Atmos. Chem. Phys. 23, 15011–15038, https://doi.org/10.5194/acp-23-15011-2023, 2023.

Yuan, T., and Oreopoulos, L.:On the global character of overlap between low and high clouds. Geophys. Res. Lett. 40(19): 5320-5326, https://doi.org/10.1002/grl.50871, 2013.

Yang, J., Ding, S., Dong, P., Bi, L., Yi, B.: Advanced radiative transfer modeling system developed for satellite data assimilation and remote sensing applications, J. Quant. Spectrosc. Radiat. Transf. 251,107043, https://doi.org/10.1016/j.jqsrt.2020.107043, 2020.

Yang, J., Zhang, Z. Q., Wei, C. Y., Lu, F., and Guo, Q.: Introducing the new generation of Chinese geostationary weather satellites, FENGYUN-4, Bull. Am. Meteorol. Soc. 98, 1637–1658, https://doi.org/10 .1175/BAMS-D-16-0065.1, 2017.

Zhao, C., Chen, Y., Li, J., Letu, H., Su, Y., Chen, T., and Wu, X.: Fifteen-year statistical analysis of cloud characteristics over China using Terra and Aqua Moderate Resolution Imaging Spectroradiometer observations. Int. J. Climatol. 39, 2612-2629, https://doi.org/10.1002/joc.5975, 2018.

Zhuge X., Zou, X., and Wang, Y.: A Fast Cloud Detection Algorithm Applicable to Monitoring and Nowcasting of Daytime Cloud Systems. IEEE Trans. Geosci. Remote. Sen. 55, 6111-6119, https://10.1109/TGRS.2017.2720664, 2017.

Zhuge, X., and Zou, X.: Summertime Convective Initiation Nowcasting over Southeastern China Based on Advanced Himawari Imager Observations. J. Meteor. Soc. Japan. Ser. II, 96(4), 337-353, https://doi.org/10.2151/jmsj.2018-041, 2018.

Zhuge, X., Zou, X., and Wang, Y.: AHI-derived daytime cloud optical/microphysical properties and their evaluations with the colletion-6.1 MOD06 Product. IEEE Trans. Geos. Remote. Sen. 59, 6431-6450, https://doi.org/10.1109/TGRS.2020.3027017, 2021.